NESS2 flat-file

MANUAL

INTRODUCTION

The new release of NESS is distributed in two '.zip' files:

- '**NESS2_flat-file.csv**' parametric table in .csv format separated by ";", containing elastic spectral acceleration ordinates (5% damped) and other Intensity Measures of ground motion with associated metadata;
- '**NESS2_flat-file_eBASCO.csv**' parametric table in .csv format separated by ";", containing elastic spectral displacement ordinates (SD) and permanent displacements of ground motion with associated metadata calculated using the extended BASeline COrrection processing (eBASCO, D'Amico et al., 2018);

Each .zip file contains the parametric table and several dictionaries ('.txt' files) explaining the abbreviations fields of the parametric tables (each dictionary has the same name as the table fields); the dictionary '**reference.txt**' contains the full citations of the references shortened in the fields named as '***_ref**'. In particular, the field '**data_source_ref**' refers to the **data_source_ref.txt** file listing the public archives to download the raw waveforms.

In the flat-files, the intensity measures (IMs) are flagged as:
- **U**: 1st component;
- **V**: 2nd component;
- **W**: 3rd component;
- **FN**: fault normal component;
- **FP**: fault parallel component;

We used U, V, W for the waveform components, as they can be oriented not only according to the North-South, East-West, and vertical directions (see http://www.fdsn.org/seed_manual/SEEDManual_V2.4.pdf, pag. 134).
FP and FN waveform components are oriented according to the fault strike and fault strike+90°, respectively.

Combinations of horizontal components of IMs are flagged as:

- **RotD50**: median value of the IMs distribution, obtained from rotated waveforms (Boore 2010);

- **RotD100**: maximum value of the IMs distribution obtained from rotated waveforms (Boore 2010);

In the following sections, we provide a brief description of the fields, grouping them as: i) event metadata; ii) source metadata; iii) station metadata; iv) source to site distances; v) waveforms metadata and vi) intensity measures.

Event metadata

- **event_id**: identifier of the event;

- **event_time**: time of the event (format YYYY-MM-DD HH:MM:SS);

- **ev_nation_code**: ISO code of the country where the epicenter of the event is located;

- **ev_latitude** and **ev_longitude**: the geographic coordinates [decimal degrees] of the epicenter of the event;

- **ev_depth_km**: depth of the hypocenter of the event [km];

- **ev_hyp_ref**: reference for **ev_latitude**, **ev_longitude** and **ev_depth_km**;

- **Mw**: moment magnitude;

- **Mw_ref**: reference for **Mw** estimate;

- **M0_foc_Nm**: seismic moment computed from the moment tensor solution [Nm];

- **M0_foc_ref**: reference for **M0_foc_Nm**;

- **stress_drop_MPa**: stress drop [MPa];

- **stress_drop_MPa_ref**: reference for **stress_drop_MPa**.

Source metadata

- **event_source_id**: identifier of the fault model; virtual fault identifier number begins with *v* (see Table 1 for computation steps of virtual fault);

- **es_nucleation_latitude** and **es_nucleation_longitude**: geographic coordinates [decimal degrees] of the starting point of the rupture on the fault plane (nucleation point);

- **es_nucleation_coord_ref**: reference for **es_nucleation_latitude** and **es_nucleation_longitude;**

- **es_nucleation_depth**: depth [km] of the of the starting point of the rupture on the fault plane (nucleation point);

- **es_nucleation_depth_ref**: reference for **es_nucleation_depth**;

- **es_strike**: fault strike [degrees from North];

- **es_dip**: fault dip [degrees];

- **es_rake**: fault rake [degrees];

- **fm_rake**: style of faulting (see dictionary);

- **es_strike_dip_rake_ref**: reference for **es_strike**, **es_dip** and **es_rake** estimates;

- **es_z_top**: depth of the fault top [km];

- **es_z_top_ref**: reference for **es_z_top** estimate;

- es_latul, es_lonul: geographic coordinates [decimal degrees] of the reference point of the fault plane;

- **es_length**: fault length [km];

- **es_width**: fault width [km];

- **es_geometry_ref**: reference for **es_length** and **es_width** estimates;

- **es_length_eff**: effective fault length from the earthquake slip model (Mai and Beroza, 2000) [km];

- **es_width_eff**: effective fault width from the earthquake slip model (Mai and Beroza, 2000) [km];

- **es_geometry_eff_ref**: reference for **es_length_eff** and **es_width_eff** estimates;

- **M0_source_Nm**: seismic moment computed from source model [Nm].

Figure 1 and Table 1 show the geometric parameters of the fault model and the procedure to compute the virtual fault, respectively.

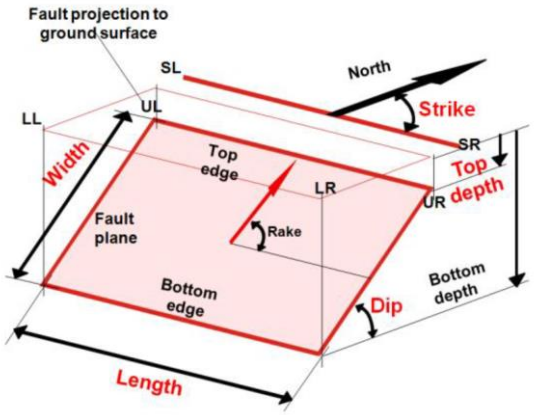

Figure 1. Geometric parameters specified for each fault model (courtesy of R. Basili).

Table 1. Steps of the procedure to define the virtual faults. UL (upper left), UR (upper right), LL (lower left), and LR (lower right) are the vertexes of the fault surface projection.

Input	Strike, dip, seismic moment, hypocentral coordinates
Step 1	Calculation of the fault length (L in km) and width (W in km) through empirical correlations in function of the moment magnitude MW (Wells and Coppersmith, 1994)
Step 2	Setting the coordinates of the nucleation points equal to epicentral ones
Step 3	Computation of the points coordinates of the fault surface projection (UR, UL, LL, LR), assuming the location of the nucleation point at 1/2 L and 2/3 W from the top edge of the fault
Step 4	Setting the depth of the nucleation point equal to the hypocentral depth. The depth of the fault plane is adjusted, assuming that the nucleation point belongs to the fault plane
Step 5	The depth of the fault top (ztop) and the fault trace, obtained from the extension of the fault plane up to surface, can be finally calculated accordingly

Station metadata

- **network_code**: code associated to the recording network according to the International Federation of Seismograph Network (http://www.fdsn.org), see dictionary for description;

- **station_code**: 3 to 5 characters associated to the station;

- **location_code**: two characters' code that identifies the sensor location (see http://www.fdsn.org/seed_manual/SEEDManual_V2.4.pdf, pag 37);

- **instrument_code**: first letter specifies the sampling rate and the response band of the instrument; the second letter specifies the family to which the sensor belongs (http://www.fdsn.org/seed_manual/SEEDManual_V2.4.pdf);

- **st_nation_code**: ISO code of the country where the station is located (see Table A1);

- **st_latitude** and **st_longitude**: geographic coordinates [decimal degrees] of the station;

- **st_elevation:** elevation of the station [m];

- **vs30_m_sec**: average shear wave velocity $V_{S,30}$ [m/s] in the uppermost 30 m estimated from in-situ measurements;

- **vs30_ref**: reference for **vs30_m_sec** estimate;

- **vs30_meas_type**: type of geophysical measurement used to estimate **vs30_m_sec** (see dictionary) from in-situ measurements.

- vs30_m_sec_WA: average shear wave velocity $V_{S,30}$ [m/s] in the uppermost 30m inferred from empirical correlation with the topographic slope, according to Wald and Allen (2007) using a 90m DEM (Digital Elevation Map provided by Shuttle Radar Topography Mission);

- ec8_code: EC8 site category (Figure 2; CEN, 2003)

- ec8_code_method: method used to estimate **ec8_code** (see dictionary);

- ec8_code_ref: reference for **ec8_code** estimate;

- NEHRP_code: NEHRP site category (Figure 3; BSSC, 2003)

- NEHRP_code_method: method used to estimate **NEHRP_code** (see dictionary);

Ground type	Description of stratigraphic profile	Parameters		
		$v_{s,30}$ (m/s)	N_{SPT} (blows/30cm)	c_u (kPa)
A	Rock or other rock-like geological formation, including at most 5 m of weaker material at the surface.	> 800	–	–
B	Deposits of very dense sand, gravel, or very stiff clay, at least several tens of metres in thickness, characterised by a gradual increase of mechanical properties with depth.	360 – 800	> 50	> 250
C	Deep deposits of dense or medium-dense sand, gravel or stiff clay with thickness from several tens to many hundreds of metres.	180 – 360	15 - 50	70 - 250
D	Deposits of loose-to-medium cohesionless soil (with or without some soft cohesive layers), or of predominantly soft-to-firm cohesive soil.	< 180	< 15	< 70
E	A soil profile consisting of a surface alluvium layer with v_s values of type C or D and thickness varying between about 5 m and 20 m, underlain by stiffer material with v_s > 800 m/s.			
S_1	Deposits consisting, or containing a layer at least 10 m thick, of soft clays/silts with a high plasticity index (PI > 40) and high water content	< 100 (indicative)	–	10 - 20
S_2	Deposits of liquefiable soils, of sensitive clays, or any other soil profile not included in types A – E or S_1			

Figure 2. EC8 ground types (Table 1.2.3 from EUR 25204 EN – 2012, CEN 2003).

3.5.1 Site Class definitions. The Site Classes are defined as follows:

A Hard rock with measured shear wave velocity, $\bar{v}_s$ > 5,000 ft/sec (1500 m/s)

B Rock with 2,500 ft/sec < $\bar{v}_s$ ≤ 5,000 ft/sec (760 m/s < $\bar{v}_s$ ≤ 1500 m/s)

C Very dense soil and soft rock with 1,200 ft/sec < $\bar{v}_s$ ≤ 2,500 ft/sec (360 m/s < $\bar{v}_s$ ≤ 760 m/s) or with either $\bar{N}$ > 50 or $\bar{s}_u$ > 2,000 psf (100 kPa)

D Stiff soil with 600 ft/sec ≤ $\bar{v}_s$ ≤ 1,200 ft/sec (180 m/s ≤ $\bar{v}_s$ ≤ 360 m/s) or with either 15 ≤ $\bar{N}$ ≤ 50 or 1,000 psf ≤ $\bar{s}_u$ ≤ 2,000 psf (50 kPa ≤ $\bar{s}_u$ ≤ 100 kPa)

E A soil profile with $\bar{v}_s$ < 600 ft/sec (180 m/s) or with either

$\bar{N}$ < 15, $\bar{s}_u$ < 1,000 psf, or any profile with more than 10 ft (3 m) of soft clay defined as soil with PI > 20, w ≥ 40 percent, and s_u < 500 psf (25 kPa)

Figure 3. NEHRP ground types (Section 3.5.1 from BSSC, 2003).

Source to site distance metrics

- **epi_dist**: epicentral distance [km];

- **epi_az**: event-to-station azimuth [degrees];

- **nucl_epi_dist**: distance from the projection of the starting point of the rupture on the fault plane [km] (nucleation point distance). If the source model does not provides information, the nucleation point is located at mid-length and at 2/3 of the fault width assuming a bilateral rupture propagation;

- **JB_dist**: Joyner-Boore distance [km];

- **rup_dist**: shortest distance from the rupture plane [km];

- **Rx_dist** and **Ry0_dist**: R_X and R_{Y0} hanging/footwall distances [km], calculated according to Ancheta et al. (2014);

- **Rline**: shorter distance from the top edge of rupture plane [km];

- **JB_dist_eff**: Joyner-Boore distance [km] considering **es_length_eff** and **es_width_eff** as fault dimensions;

- **rup_dist_eff**: distance from the rupture plane [km] considering **es_length_eff** and **es_width_eff** as fault dimensions;

- **Rx_dist_eff** and **Ry0_dist_eff**: R_X and R_{Y0} hanging/footwall distances [km], calculated according to Ancheta et al. (2014) considering **es_length_eff** and **es_width_eff** as fault dimensions;

- **Rline_eff**: shorter distance from the top edge of rupture plane [km] considering **es_length_eff** and **es_width_eff** as fault dimensions.

Figure 4 shows how source-to-site distances are computed. In particular, the right panel illustrates the distance R_X defined to be positive for sites on the hanging-wall side of the fault and negative for sites on the footwall side of the fault. The distance R_{Y0} is zero or positive (Kaklamanos et al., 2011).

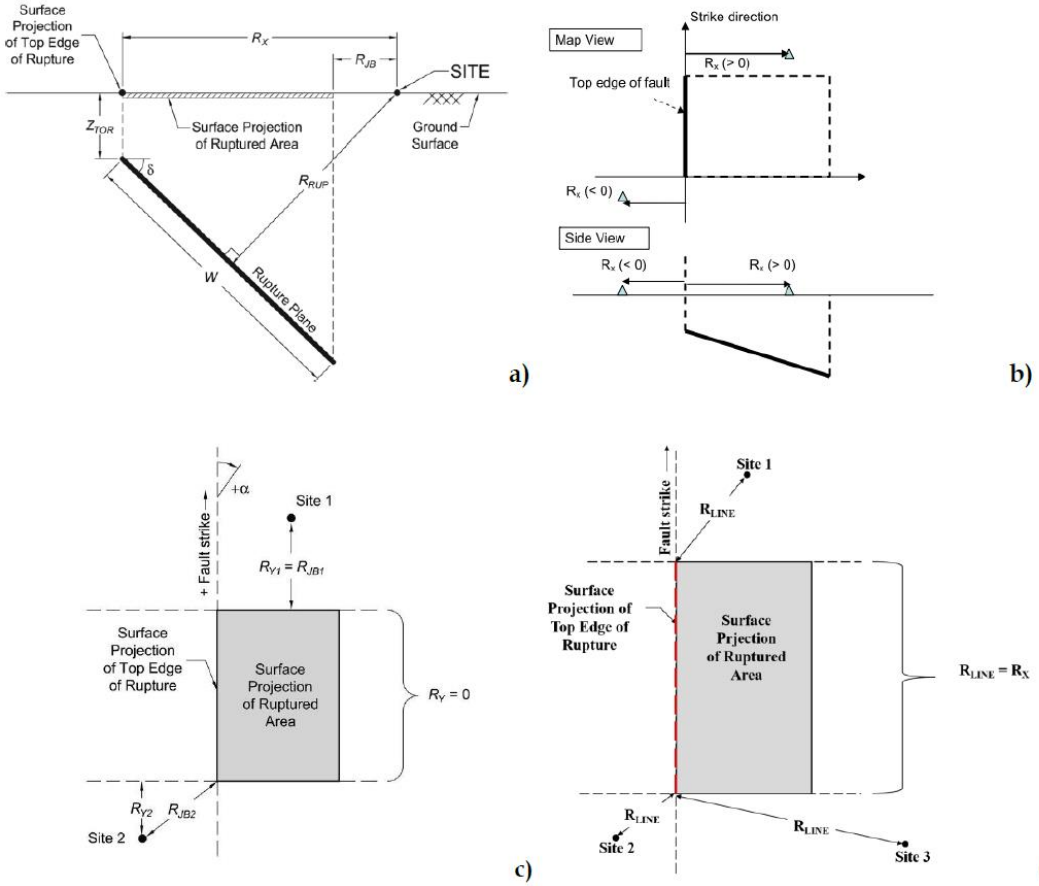

Figure 4. a) Representation of the earthquake source and distance measures using a vertical cross section through a fault rupture plane (taken from Kaklamanos et al., 2011). b) map (top) and side (bottom) view of the source-to-site distance measure (R_X) for an example fault (thick black line) plane and stations located on the hanging wall ($R_X > 0$) and footwall ($R_X < 0$) side (taken from Ancheta et al., 2013). c) map view of R_{Y0} definition. d) map view of the source-to-site distance measure RLINE for three sites located on different sides of the surface projection of the fault.

Waveform metadata

- **instrument_type_code**: 'A': analog instrument; 'D': digital instrument; 'U': unknown type of instrument;

- **late_triggered_flag_01**: flag to identify analog record starting with the S-phase (Puglia et al., 2018; Paolucci et al., 2011);

- ***X*_channel_code**: channel code of the *X* component according to the SEED convention http://www.fdsn.org/seed_manual/SEEDManual_V2.4.pdf, pag. 134);

- ***X*_azimuth_deg**: azimuth of the *X* component from the North [degrees];

- ***X*_hp**: high-pass frequency [Hz] of the Butterworth filter (2nd order) of the *X* component according to the processing schema described in Puglia et al. (2018) and Paolucci et al (2011);

- ***X*_lp**: low-pass frequency [Hz] of the Butterworth filter (2nd order) of the *X* component according to the processing schema described in Puglia et al. (2018)

and Paolucci et al (2011);

Where *X* component is *U*, *V* and *W*.

The '**NESS2_flat-file_eBASCO.csv**' parametric table also contains the following fields according to D'Amico et al. (2019):

- **processing_type** of eBASCO processing (0: automatically processed; 1: manually processed)

- **T1_samples**: number of samples for the T1 correction points;

- **T2_samples**: number of samples for the T2 correction points;

- **T3_samples**: number of samples for the T3 correction points;

- **eps**: maximum threshold of the relative difference between acceleration in T1 and T2 correction point before and after the eBASCO processing;

- **mfst**: multiplier factor to cut the beginning of the waveform on the base of the energy criterion;

- **mfnd**: multiplier factor to cut the end of the waveform on the base of the energy criterion;

- **ca_sec**: seconds to cut from the beginning of the waveforms; *ca_sec* is used only if it is different from the default value, otherwise eBASCO use the energy criterion to cut the strong-phase of motion between the 5% and the 95% of the energy release;

- **cz_sec**: seconds to cut from the end of the waveforms; *cz_sec* is used only if it is different from the default value, otherwise eBASCO use the energy criterion to cut the strong-phase of motion between the 5% and the 95% of the energy release;

- **ta**: percentage of the signal length to set the time window at the beginning of the waveform where a cosine taper will be applied.

Intensity measures

- ***X*_pga**: peak ground acceleration [cm/s^2];

- ***X*_pgv**: peak ground velocity [cm/s];

- ***X*_pgd**: peak ground displacement [cm];

- ***X*_pds**: permanent displacement [cm] provided only in 'NESS2_flat-file_eBASCO.csv' parametric table;

- ***X*_T90**: duration [s] of the time interval between the points of 5% and 95% of the total energy (Trifunac and Brady, 1975);

- ***X*_housner**: Housner intensity [cm];

- ***X*_CAV**: Cumulative Absolute Velocity [cm/s];

- ***X*_ia**: Arias intensity [cm/s];

- **pulse_like**: pulse like behavior (see dictionary);

- **pulse_azimuth**: the azimuthal direction along which the pulse is observed [degrees];

- **Tp**: pulse period [s] defined as the pseudo-period of the wavelet extracted following the procedure developed by Baker (2007) and by Shahi and Baker (2014);

- ***X*_Ty_yyy**: acceleration response spectra (5% damping, cm/s^2) for 36 periods between 0.01s and 10s;

where:

- *X* component is *U*, *V*, *W*, *FN*, *FP, RotD50, RotD100*;
- y_yyy identifies the period corresponding to the spectral ordinate (where the character '_' indicates the decimal point, e.g. 0_100 corresponds to T=0.100s).

In the '**NESS2_flat-file_eBASCO.csv**' parametric table ***X*_Ty_yyy** fields are computed with reference to linear displacement response spectra 5% damped (cm) for 36 periods between 0.01s and 10s;

References

Ancheta TD, Darragh RB, Stewart JP, Seyhan E, Silva WJ, Chiou BSJ, Wooddell KE, Graves RW, Kottke AR, Boore DM, Kishida T (2014). NGA-West2 database. Earthquake Spectra, 30(3), 989-1005.

Baker J.W. (2007) Quantitative classification of near-fault ground motions using wavelet analysis, Bulletin of the Seismological Society of America, 97 (5), 1486- 1501.

Boore DM (2010). Orientation-independent, nongeometric-mean measures of seismic intensity from two horizontal components of motion. Bulletin of the Seismological Society of America, 100(4), 1830-1835.

D'Amico M., Felicetta C., Schiappapietra E., Pacor F., Gallovic F., Paolucci R., Puglia R., Lanzano G., Sgobba S., Luzi L. (2019) Fling Effects from Near-Source Strong-Motion Records: Insights from the 2016 Mw 6.5 Norcia, Central Italy, Earthquake. Seismological Research Letters Volume 90, Number 2A. doi: 10.1785/0220180169

CEN (2003). EuroCode 8: Design of structures for earthquake resistance—Part 1: General rules, seismic actions and rules for buildings. Bruxelles: European Committee for Standardization.

BSSC (2003) NEHRP recommended provisions for seismic regulations for new buildings and other structures (fema 450)

Kaklamanos, J., Baise, L.G., Boore, D.M. (2011). Estimating unknown input parameters when implementing the NGA ground-motion prediction equations in engineering practice. Earthquake Spectra, 27 (4), 1219-1235.

Mai, P. M., and G.C. Beroza (2000). Source scaling properties from finite-fault-rupture models. Bulletin of the Seismological Society of America, 90(3), 604-615.

Paolucci R, Pacor F, Puglia R, Ameri G, Cauzzi C, Massa M (2011) Record processing in ITACA, the new Italian strong-motion database. In: Akkar S, Gulkan P, van Eck T (eds) Chapter 8 of the book earthquake data in engineering seismology—predictive models, data management and networks. ISBN: 978-94-007-0151-9 (printed version) 978-94-007-0152-6 (E-book version). Geotechnical, geological, and earthquake engineering, vol 14, Springer, Netherlands

Puglia, R., Russo, E., Luzi, L., D'Amico, M., Felicetta, C., Pacor, F., & Lanzano, G. (2018). Strong-motion processing service: A tool to access and analyse earthquakes strong-motion waveforms. Bulletin of Earthquake Engineering, 16(7), 2641-2651.

Shahi, S.K. and Baker, J.W. (2014) An efficient algorithm to identify strong velocity pulses in multi-component ground motions. Bulletin of the Seismological Society of America, 104(5), 2456-2466.

Trifunac MD, Brady AG (1975). A study on the duration of strong earthquake ground motion. Bulletin of the Seismological Society of America, 65(3), 581-626.

Wald DJ, Allen TI (2007). Topographic slope as a proxy for seismic site conditions and amplification. Bulletin of the Seismological Society of America, 97(5), 1379-1395.

Wells, DL, and Coppersmith, KJ (1994). New empirical relationships among magnitude, rupture length, rupture width, rupture area, and surface displacement. Bulletin of the seismological Society of America, 84(4), 974-1002.